

Hierarchical porous CsPbBr₃@HZIF-8 heterojunction for high-performance photocatalytic degradation of antibiotics in high-salinity wastewater

Yangwen Hou,^a Fanfei Meng,^b Jingting He,^a Man Dong,^c Jialin Tong,^c Jing Sun,^b Chunyi Sun,^{*c} Xinlong Wang,^c and Zhongmin Su^{*b,d}

^aSchool of Materials Science and Engineering, Changchun University of Science and Technology, Changchun 130022, China

^bJilin Provincial Science and Technology Innovation Center of Optical Materials and Chemistry, School of Chemistry and Environmental Engineering, Changchun University of Science and Technology Changchun, Changchun, 130022 Jilin, China

^cKey Laboratory of Polyoxometalate Science of Ministry of Education, Northeast Normal University, Changchun, 130024 Jilin, China

^dState Key Laboratory of Supramolecular Structure and Materials, Institute of Theoretical Chemistry, College of Chemistry, Jilin University, Changchun 130021, China

* Corresponding author.

E-mail addresses: suncy009@nenu.edu.cn (C. Sun), zmsu@nenu.edu.cn (Z. Su).

1. Experimental Section

1.1 Chemical Reagents

Zinc nitrate hexahydrate (Zn(NO₃)₂·6H₂O, 99.0%), Zinc sulfate heptahydrate (ZnSO₄·7H₂O, AR), 2-Methylimidazole (C₄H₆N₂, 98.0%), lead bromide (PbBr₂, 99.9%), cesium bromide (CsBr, 99.0%), oleic acid (OA, 80%-90%), oleylamine (OAm, 90.0%), Dimethyl sulfoxide (DMSO, C₂H₆SO, >99.0%), toluene (C₇H₈, 99.0%), N, N-dimethylformamide (DMF, C₃H₇NO, 99.5%), methanol (CH₃OH, 99.5%), ethanol (CH₃CH₂OH, 99.5%), Tetracycline hydrochloride (C₂₂H₂₄N₂O₈·HCl, 96%), L-Histidine (C₆H₉N₃O₂, > 99.0%), triethanolamine (TEOA, C₆H₁₅NO₃, 98.0%), benzoquinone (BQ, C₆H₄O₂, 99.0%), and isopropyl alcohol (IPA, C₃H₈O, 98.0%) were purchased from Aladdin Co. Ltd.

1.2 Characterization.

Powder X-ray diffraction (PXRD) analysis was conducted using an X-ray diffractometer (Rigaku, Japan) equipped with Cu K α radiation. Transmission electron microscopy (TEM) images were acquired using JEOL, JEM-2100F. The surface morphology of the fabricated material were examined using scanning electron microscopy (SEM) with a FEI Quanta 600 instrument. UV-visible diffuse reflectance spectroscopy (UV-Vis DRS) measurements were carried out using a Shimadzu UV-2600 UV-visible spectrophotometer (Japan). X-ray photoelectron spectroscopy (XPS) analysis was conducted using a Thermo ESCALAB 250Xi instrument with Al K α X-ray radiation. Ultraviolet photoelectron spectroscopy (UPS) was carried out by X-ray photoelectron spectroscopy (PHI5000 VersaProbe III). FTIR spectra were obtained using an attenuated total reflectance (ATR) mode on a Nicolet iS 50 instrument (Thermo Fisher, USA). Photoluminescence (PL) emission spectra were collected using a fluorescence spectrophotometer (F7000, Hitachi, Japan). Time-resolved photoluminescence (TRPL) spectra were recorded on a fluorescence lifetime spectrophotometer (FLS 1000, Edinburgh, UK) with an excitation wavelength of 325 nm. Electrochemical measurements were performed using an electrochemical analyzer (CHI660C, CH Instruments,

Shanghai). The counter electrode, reference electrode, and electrolyte used in the measurements were Pt wire, Ag/AgCl (saturated KCl), and a 0.5 M Na₂SO₄ solution, respectively.

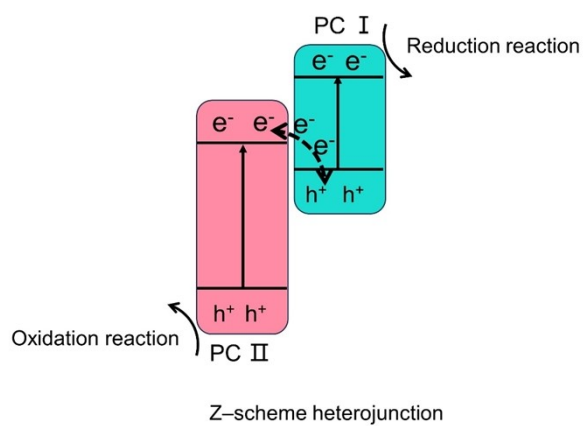


Fig.S1. Schematic illustration of charge carrier transfer in direct Z-scheme photocatalysts (this work).

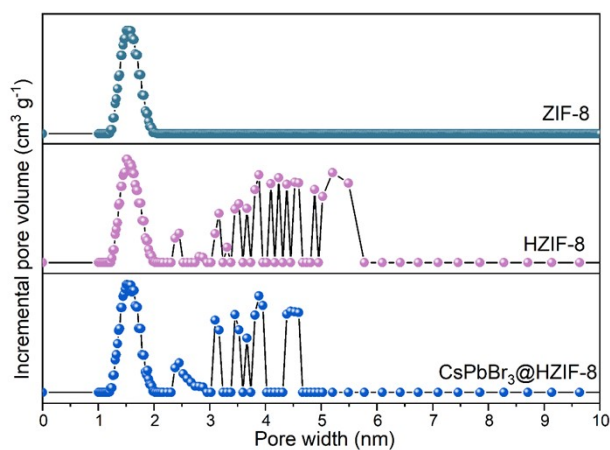


Fig.S2. Pore size distributions based on density-functional theory (DFT) analysis of ZIF-8 and HZIF-8 and CsPbBr₃@HZIF-8.

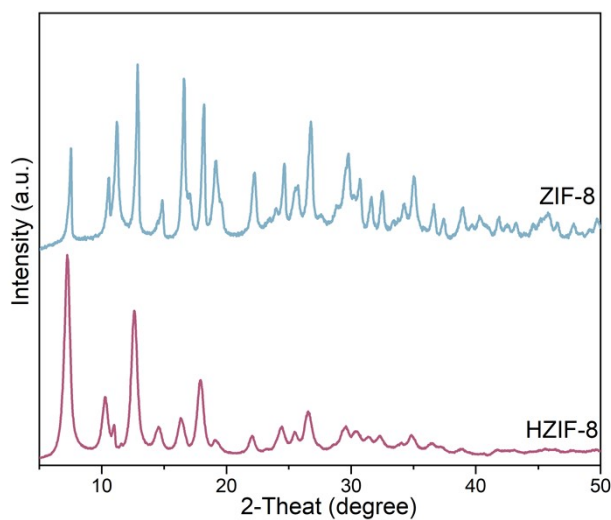


Fig.S3. PXRD patterns of ZIF-8 and HZIF-8.

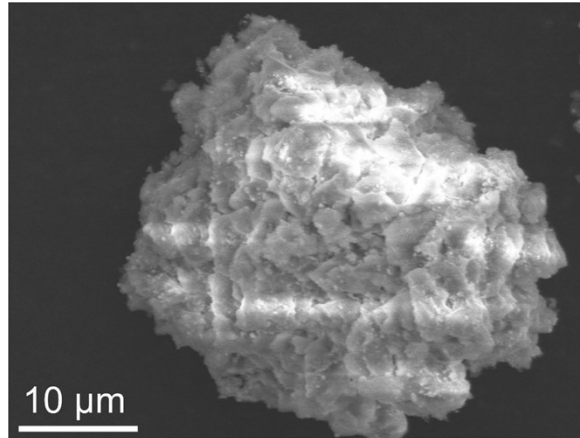


Fig.S4. SEM of 4%-CsPbBr₃@HZIF-8.

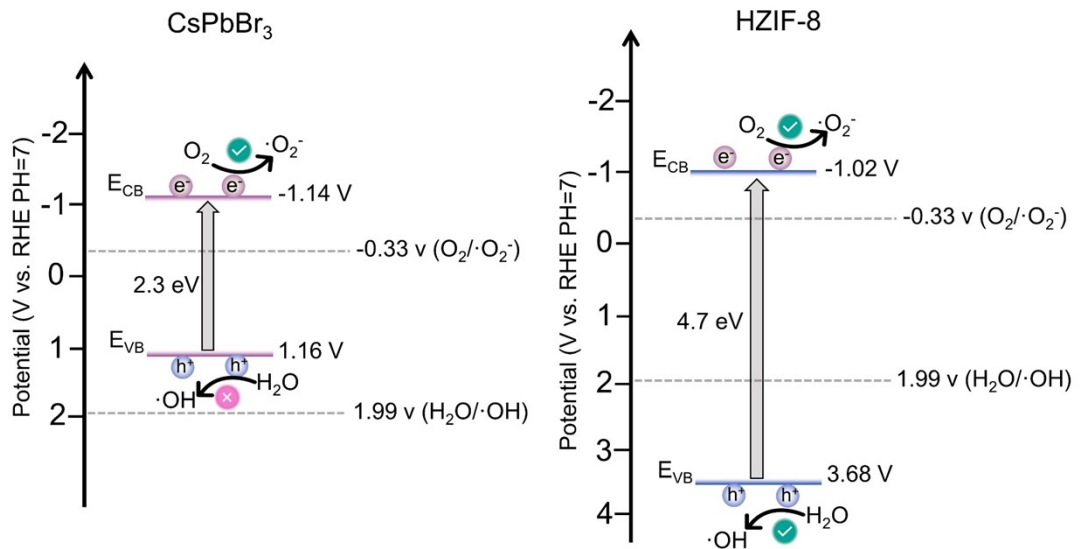


Fig.S5. Band structures of CsPbBr₃ and HZIF-8 from UPS.

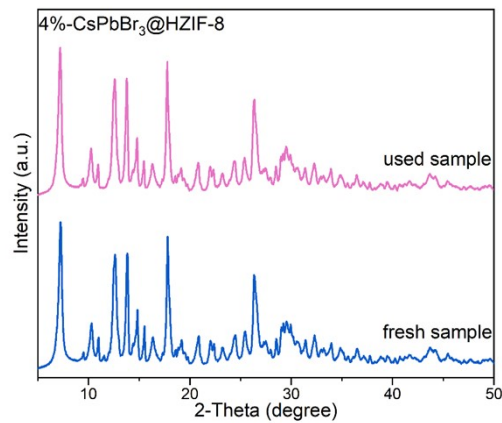


Fig.S6. Post-reaction PXRD of 4%-CsPbBr₃@HZIF-8.

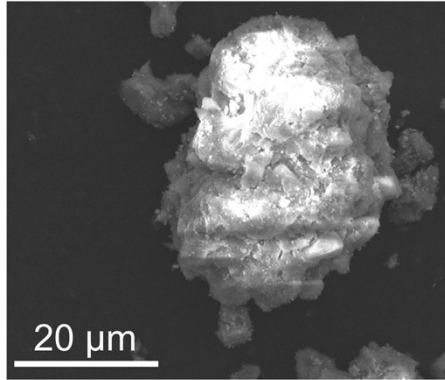


Fig. S7. Post-reaction SEM images of 4%-CsPbBr₃@HZIF-8.

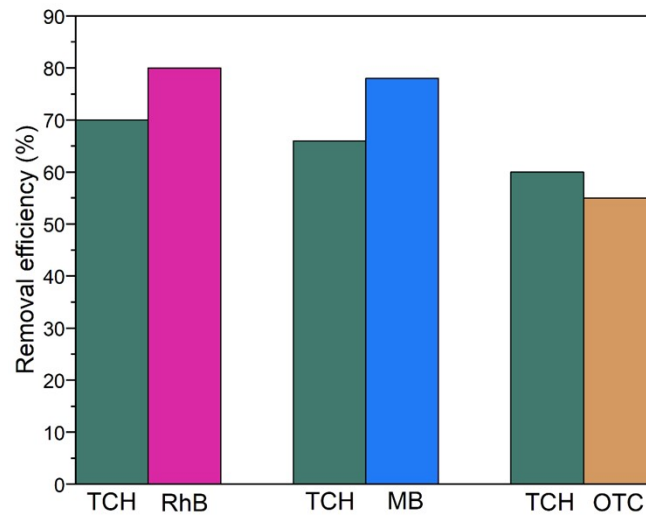


Fig.S8. 4%-CsPbBr₃@ZIF-8 for degradation of pollutants in the coexistence system.

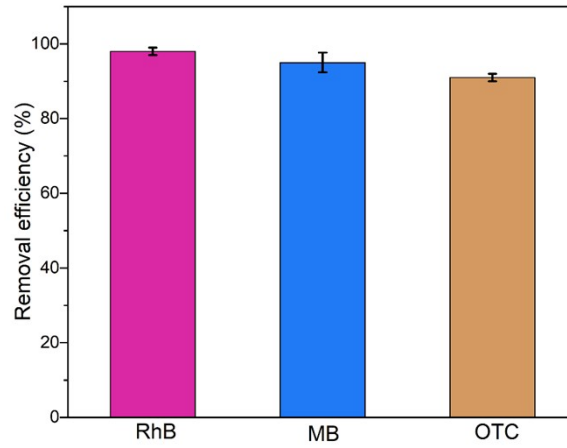


Fig.S9. 4%-CsPbBr₃@ZIF-8 for degradation of different pollutants.

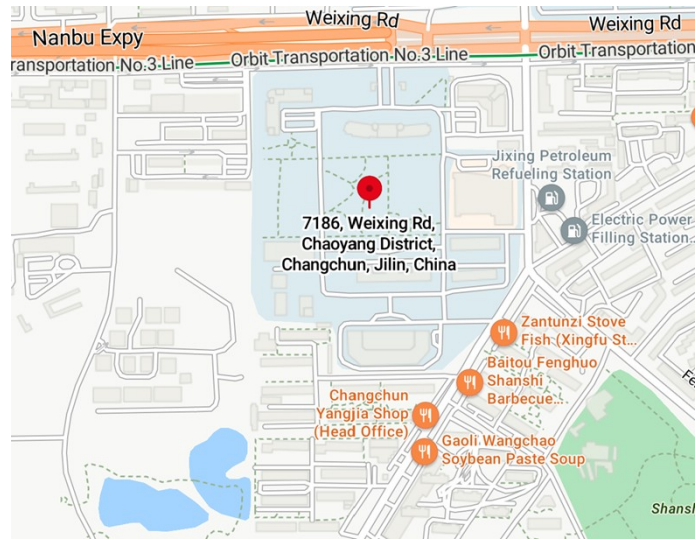


Fig. S10. Map of tap water sources.

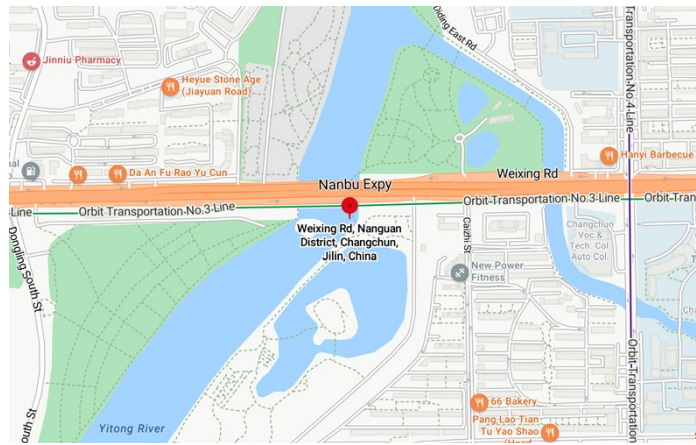


Fig.S11. Map of river sources.

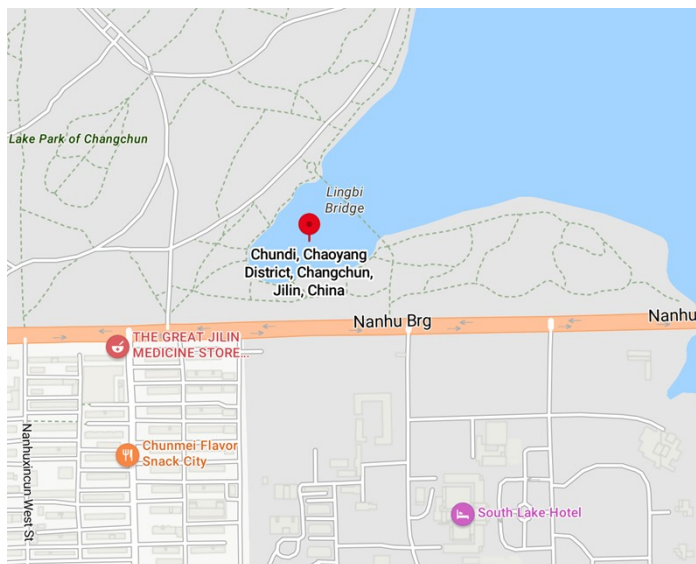
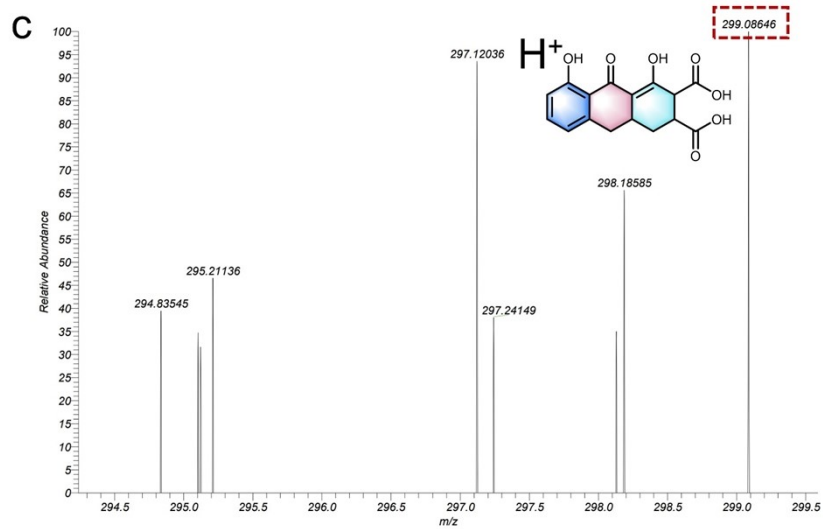
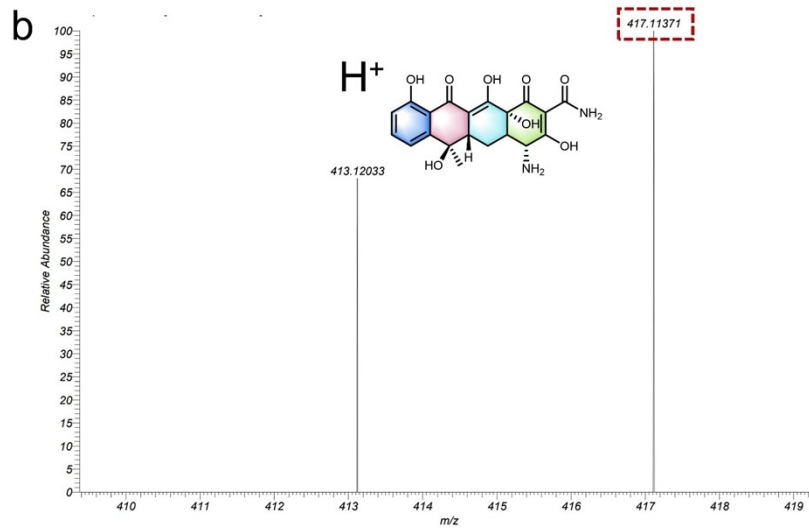
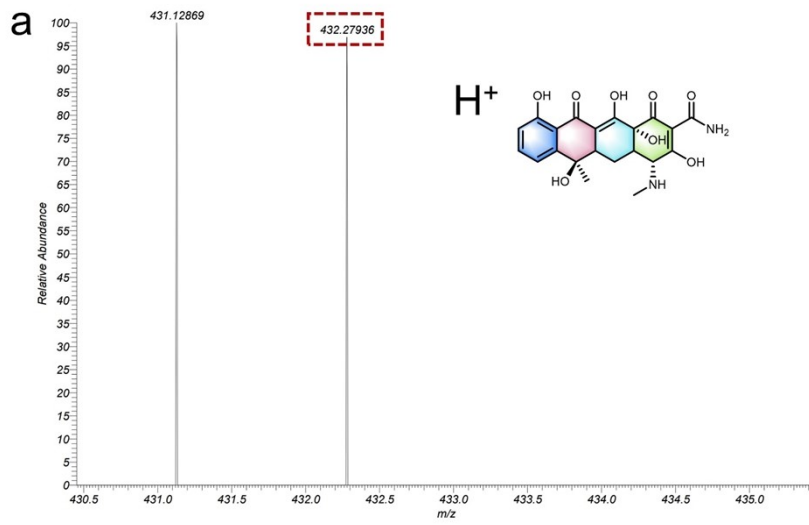
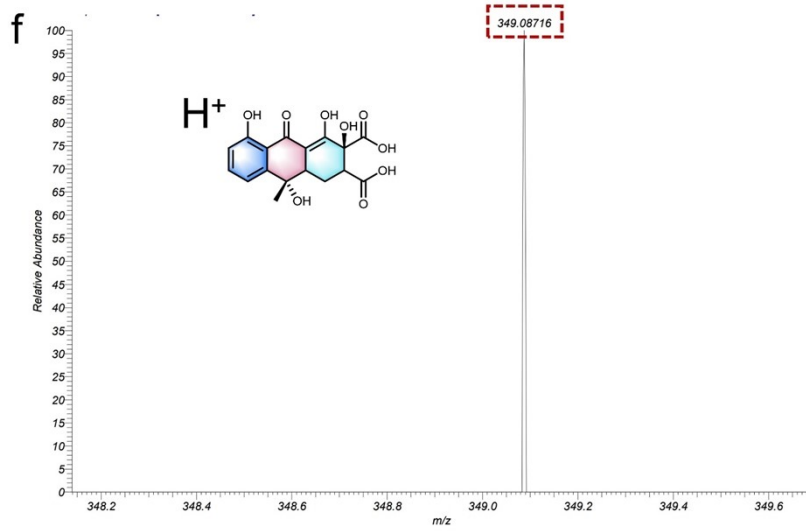
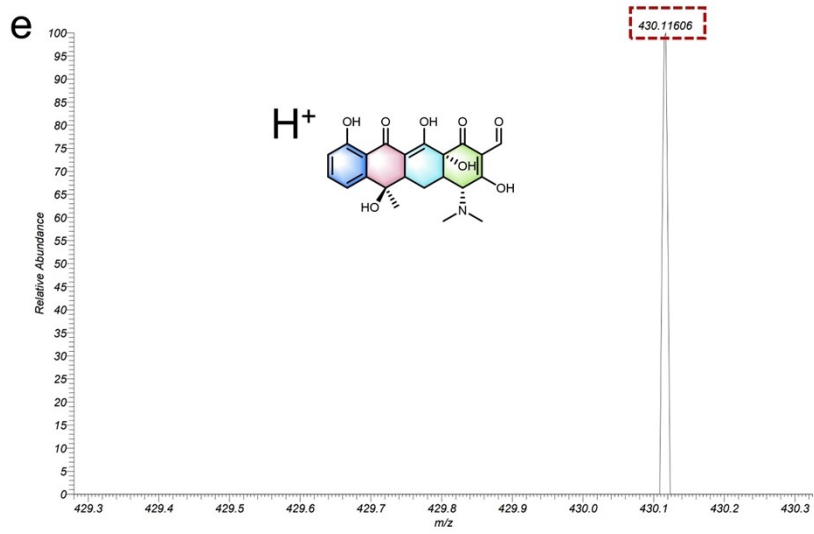
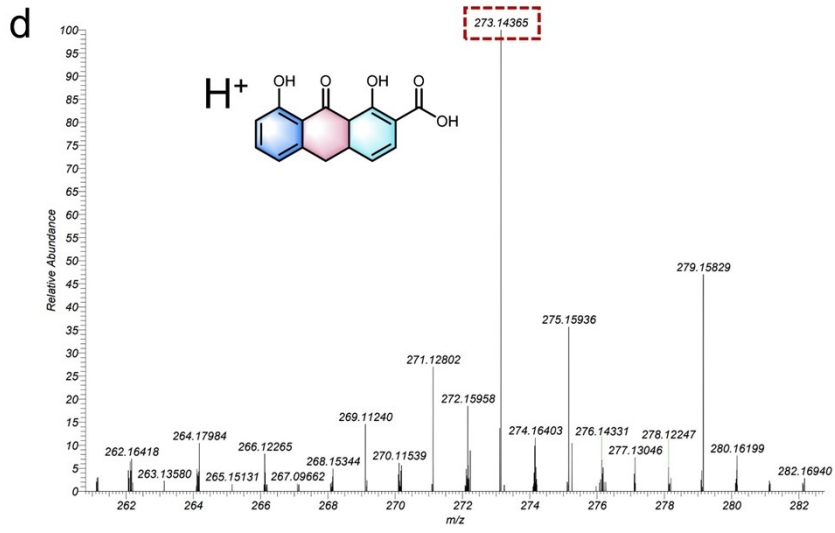


Fig.S12. Map of lake sources.





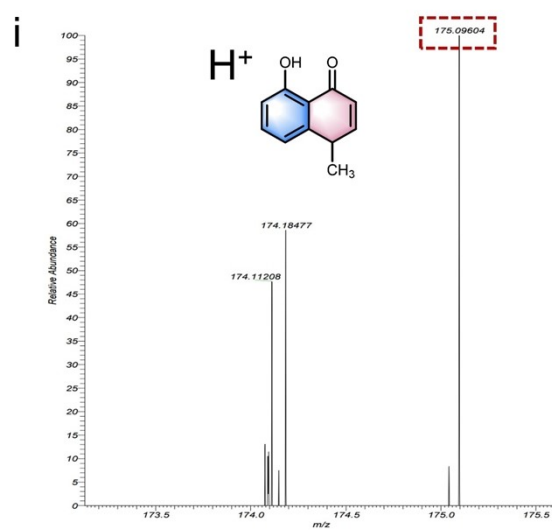
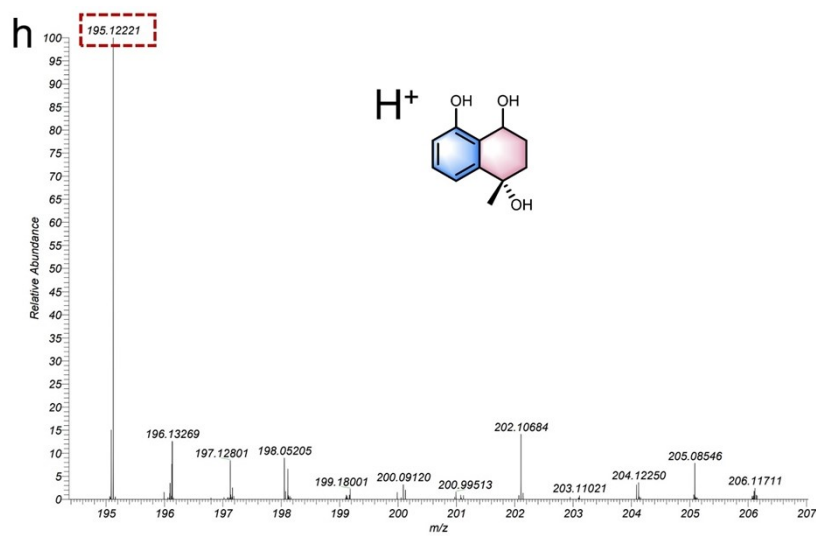
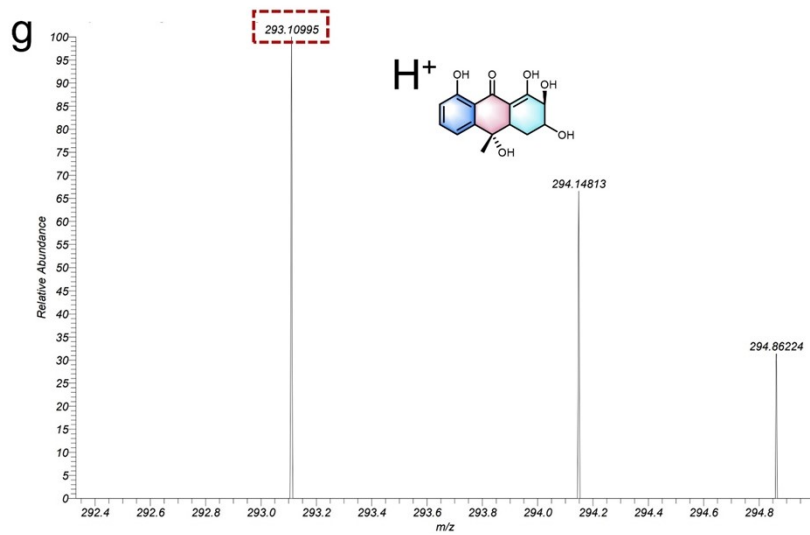


Fig. S13. Spectra of degradation intermediates (a-I, P1-P9).

Table S1. Photocatalytic degradation of TCH by various photocatalysts.

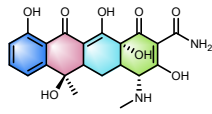
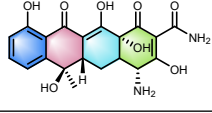
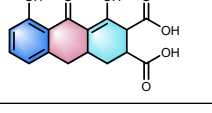
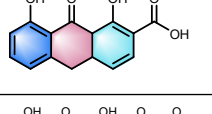
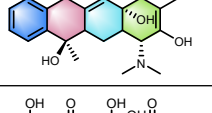
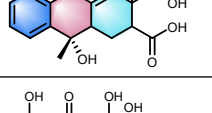
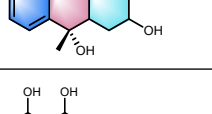
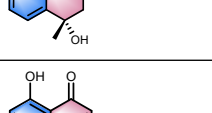
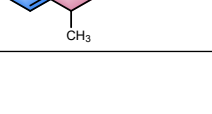
Photocatalyst (amount)	Organics (Concentration)	Irradiation time	Light source	Degradatio n	
CsPbBr ₃ @HZIF-8 (15 mg)	30 mL TCH (10 mg/L)	40 min	300W Xe-lamp ($\lambda > 420$ nm)	94%	This work
CsPbBr ₃ -TiO ₂ (50 mg)	100 mL TCH (20 mg/L)	60 min	300W Xe-lamp ($\lambda > 420$ nm)	94%	1
CsPbBr ₃ @SiO ₂ (50 mg)	100 mL TCH (20 mg/L)	120 min	300W Xe-lamp ($\lambda > 420$ nm)	75%	2
CsPbBr ₃ QDs (100 mg)	100 mL TCH (10 mg/L)	30 min	300W Xe-lamp ($\lambda > 420$ nm)	76%	3
ZIS@P20 (8 mg)	40 mL TCH (20 mg/L)	60 min	800W Xe-lamp ($\lambda > 420$ nm)	99.9%	4
N-CNT/mpg-C ₃ N ₄ (50 mg)	50 mL TCH (20 mg/L)	240 min	300W Xe-lamp ($\lambda > 420$ nm)	67.1%	5
γ -Fe ₂ O ₃ /g-C ₃ N ₄ (50 mg)	100 mL TCH (10 mg/L)	120 min	500W Xe-lamp ($\lambda > 420$ nm)	73.8%	6
Bi ₂ Sn ₂ O ₇ / Bi ₂ MoO ₆ (25 mg)	100 mL TCH (20 mg/L)	100 min	300W Xe-lamp ($\lambda > 400$ nm)	98.7%	7

Table S2 Time-resolved PL decay parameters of different samples under 365 nm excitation. The two-exponential decay curves were fitted using a non-linear least-squares method with a two-component decay law. The average lifetime (τ_{av}) was then determined using the equation:

$$\tau = \frac{\sum_{i=1}^{i=n} A_i \tau_i^2}{\sum_{i=1}^{i=n} A_i \tau_i}$$

τ_1 (ns)	τ_2 (ns)	χ^2	τ_{av} (ns)
14.59 (17.70%)	46.69 (82.30.2%)	1.077	40.99
7.94 (5.23%)	29.48 (94.77%)	1.053	28.35

Table S3 Characteristics of intermediate products of the degradation of TCH.

Name	m/z	Supposed Structure
P1	431	
P2	416	
P3	298	
P4	272	
P5	429	
P6	348	
P7	292	
P8	194	
P9	174	

References

- 1 C. Liu, X. Qian, Q. Wei, Z. Chen, J. Chen, W. Wang, X. Chen, J. Gao, Y. Liu and L. Xie, *J. Clean. Prod.*, 2022, **365**, 132830.
- 2 J. Gao, X. Qian, Q. Wei, Z. Chen, C. Liu, W. Wang, J. Chen, X. Chen, Y. Liu and G. Wei, *J. Colloid Interface Sci.*, 2022, **623**, 974–984.
- 3 X. Qian, Z. Chen, X. Yang, W. Zhao, C. Liu, T. Sun, D. Zhou, Q. Yang, G. Wei and M. Fan, *J. Clean. Prod.*, 2020, **249**, 119335.
- 4 P. Jin, L. Wang, X. Ma, R. Lian, J. Huang, H. She, M. Zhang and Q. Wang, *Appl. Catal. B*, 2021, **284**, 119762.
- 5 J. Liu, Y. Song, H. Xu, X. Zhu, J. Lian, Y. Xu, Y. Zhao, L. Huang, H. Ji and H. Li, *J. Colloid Interface Sci.*, 2017, **494**, 38–46.
- 6 C. Li, S. Yu, H. Che, X. Zhang, J. Han, Y. Mao, Y. Wang, C. Liu and H. Dong, *ACS Sustain. Chem. Eng.*, 2018, **6**, 16437–16447.
- 7 S. Li, C. Wang, Y. Liu, M. Cai, Y. Wang, H. Zhang, Y. Guo, W. Zhao, Z. Wang and X. Chen, *Chem. Eng. J.*, 2022, **429**, 132519.